

## Magnetic properties of Co/GaAs(110)

T. L. Monchesky<sup>1,2</sup> and J. Unguris<sup>2</sup>

<sup>1</sup>*Department of Physics and Atmospheric Science, Dalhousie University, Halifax NS, Canada B3H 3J5*

<sup>2</sup>*Electron Physics Group, National Institute of Standards and Technology, Gaithersburg, Maryland 20899-8412, USA*

(Received 1 August 2006; revised manuscript received 30 October 2006; published 4 December 2006)

We observed three magnetic states of an ultrathin, atomically well-ordered Co film grown on a cleaved GaAs(110) substrate. For a Co thickness less than 3.4 monolayers (ML), we find a ferromagnetically dead layer associated with the formation of interfacial Co<sub>2</sub>GaAs. For thicknesses greater than 4.1 ML, the Co film grows with a bcc structure that contains 6 at. % Ga. The films are ferromagnetic with an easy axis along the  $[\bar{1}10]$  direction. This magnetic state persists up to a thickness of 7 ML, at which point an abrupt in-plane spin-reorientation transition reorients the magnetization along the [001] direction.

DOI: [10.1103/PhysRevB.74.241301](https://doi.org/10.1103/PhysRevB.74.241301)

PACS number(s): 75.70.Ak, 75.30.Kz, 75.70.Kw, 81.30.Kf

Growth of ultrathin films by molecular beam epitaxy (MBE) provides a means of creating new phases of matter with crystal structures that would not otherwise exist in nature. Examples of this type of atomic engineering include Ni<sup>1</sup> and Co grown on GaAs. Bulk Co prefers to form a hcp phase at room temperature, but when grown epitaxially on GaAs(110), Co forms into a bcc structure that is stable up to thicknesses as large as 175 ML, depending on the substrate and growth conditions.<sup>2-4</sup> bcc-Co is especially interesting since its majority spin-band is nearly completely filled.<sup>5-7</sup> This property makes it particularly attractive as an electrode for spintronic devices.<sup>8,9</sup>

Until now, the details of the thickness dependence of the variations in the magnetic properties of Co/GaAs(110) have not been studied. Brillouin light scattering shows that uniaxial anisotropy dominates the total magnetocrystalline anisotropy and produces an easy axis along the [100] direction.<sup>10</sup> In addition, polarized neutron reflection (PNR) measures a reduced magnetic moment of  $1.0 \mu_B$  near the Co/GaAs interface and  $1.7 \mu_B$  near the center of the film.<sup>11</sup> A more complete understanding of the magnetic properties of thin bcc-Co films has been hindered by the difficulty of preparing high-quality films for measurement due to the reactivity of the Co/GaAs(110) system. Researchers have attempted to improve the quality of growth by passivating the GaAs(110) surface,<sup>12</sup> and by using surfactant-mediated growth.<sup>13</sup> We have focused on improving the growth by improving the quality of the substrate through the use of *in situ* cleaved, single-crystal GaAs(110), a method used successfully in earlier photoemission experiments.<sup>14</sup>

In this paper we show that crystalline Co films grown on GaAs(110) have three distinct magnetic configurations. For films less than 3.4 ML, we observe a magnetically dead phase that explains the origin of the reduced magnetic moment observed by others at the Co/GaAs interface. We show that the composition of this phase is consistent with Co<sub>2</sub>GaAs reported in Ref. 15. Above this thickness we find a Co-Ga component with a bcc structure. At a thickness of 7 ML, we observe a spin reorientation. Observation of this new spin reorientation was enabled by improving the epitaxial order of the Co growth on the GaAs surface. Unlike previous studies, which used mechanically polished wafers, we grew the Co on cleaved GaAs surfaces, which provided more

atomically well-ordered growth substrates. Furthermore, wedge-shaped Co samples were deposited *in situ* in the ultrahigh-vacuum electron microscope, which allowed us to study the evolution of the Co film in submonolayer detail. Magnetic, structural, and chemical properties were measured as a function of Co film thickness using scanning electron microscopy with polarization analysis (SEMPA), reflection electron microscopy, and scanning auger microscopy, respectively.

High-quality, clean GaAs(110) surfaces were prepared by cleaving 0.5-mm-thick wafers in a base pressure of  $2 \times 10^{-7}$  Pa. The samples were then immediately transferred to the analysis/growth chamber, where the base pressure was  $2 \times 10^{-8}$  Pa. Reflection high-energy electron diffraction (RHEED) patterns from the GaAs(110) surface indicated very high quality surfaces with sharp diffraction spots distributed on a Laue circle, without any visible streaks (see Fig. 1). Scanning tunneling microscopy measurements of similarly prepared surfaces indicated that the sample was atomically flat over regions that were micrometers wide.

Cobalt from an electron beam evaporator was deposited onto the room temperature GaAs surface at a rate of typically  $1.7 \times 10^{-2}$  ML/s. The pressure did not rise above  $3.8 \times 10^{-8}$  Pa during the growth. A retractable shutter, placed 20  $\mu\text{m}$  above the substrate surface, was scanned in front of the substrate during evaporation, creating a Co wedge that varied linearly in thickness from 0 ML to 30 ML along the  $[\bar{1}10]$  direction. The slope of different wedges varied from 0.045 ML/ $\mu\text{m}$  to 0.12 ML/ $\mu\text{m}$ . Here 1 ML corresponds to a surface density of  $1.77 \times 10^{19} \text{ m}^{-2}$ . RHEED oscillations (see Fig. 2) persisted beyond 30 ML and showed that Co grew in a near layer-by-layer fashion on GaAs(110). Spatially resolved RHEED intensity oscillations were imaged using the scanning electron microscope,<sup>16</sup> and the relative Co film thickness at every point along the wedge sample was determined to within  $\pm 0.15$  ML.

RHEED images, shown in Fig. 1, were recorded along the wedge to monitor the crystal structure as a function of thickness. At a thickness of 2.8 ML, the RHEED image in Fig. 1(b) began to show streaks due to the short terraces of the film. A well-defined splitting of the RHEED streaks indicated the existence of a well-defined terrace size. The splitting of 2.0 nm<sup>-1</sup> gave a crude estimate of the characteristic terrace

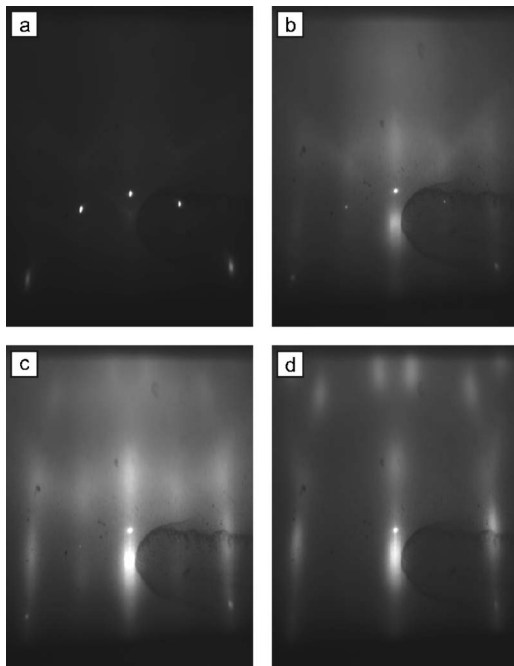


FIG. 1. (a) RHEED images with the electron beam parallel to  $[001]$ : (a) clean GaAs(110) substrate, (b) 2.8 ML, (c) 5.7 ML, and (d) 8.9 ML of Co on GaAs(110).

length of 6 nm. At a thickness of 5.7 ML, the RHEED pattern in Fig. 1(c) is consistent with a bcc lattice. Superimposed on the typical bcc pattern are half-order streaks likely due to the CoAs on the surface. Additional diffuse diffraction spots appeared in the RHEED images as the thickness increased. Similar patterns were reported in the literature and were attributed to the formation of an hcp phase.<sup>17</sup> The thickness at which this phase change occurred varied from sample-to-sample, from about 5 ML to 8 ML. This transition thickness was much lower than the transition thickness reported by others.<sup>4</sup> We suggest that the high surface quality of cleaved surfaces used in this study was not rough enough to stabilize the bcc phase at larger thicknesses. The spots associated with the hcp phase were more intense at lower incident beam angles, suggesting that this second phase is only present at the surface.

Three distinct magnetic states are revealed by the SEMPA images of the two in-plane magnetization components shown in Fig. 2: a nonmagnetic phase, a ferromagnetic phase with an easy axis along the  $[\bar{1}10]$ , and a ferromagnetic phase with an easy axis along  $[001]$ . No out-of-plane magnetization component was observed. To obtain a quantitative measure of the spin polarization as a function of thickness, line scans of the magnitude of the magnetization components along the wedge were obtained from the images and then averaged across the images. Instrumental polarization offsets were determined and removed from the line scans by repeating the SEMPA measurements after applying magnetic fields along the  $[001]$  and  $[\bar{1}10]$  directions to reverse the direction of the magnetic domains. The resulting line scans are shown in Fig. 3. These data clearly reveal a magnetically dead film up to a thickness of  $t_{\text{onset}} = 4.1 \text{ ML} \pm 0.2 \text{ ML}$ . Above  $t_{\text{onset}}$  we observed a ferromagnetic phase with uniaxial magnetocrystal-

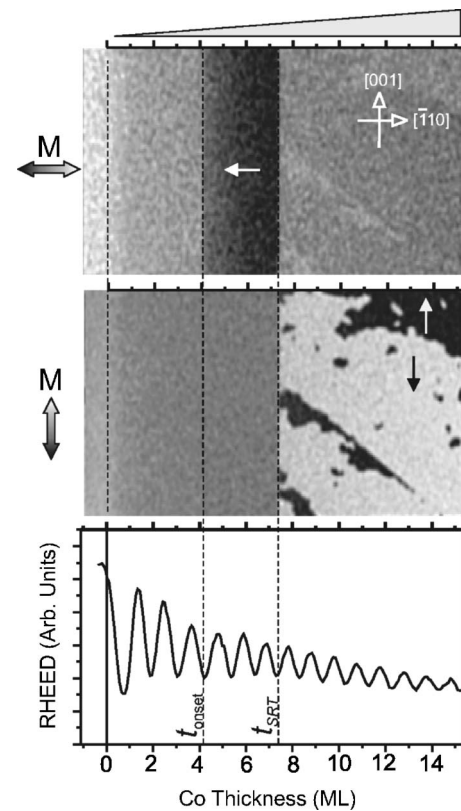


FIG. 2. Top and middle:  $x$  and  $y$  component of a  $124 \mu\text{m} \times 73.7 \mu\text{m}$  magnetization image of a Co wedge on GaAs(110). Bottom: RHEED intensity oscillations measured along the wedge.

line anisotropy and an easy axis aligned along  $[\bar{1}10]$  to within  $\pm 5^\circ$ . The magnetization was nearly single domain across this entire phase, although a few samples had domains near substrate defects with domain walls running roughly parallel to the magnetization.

The SEMPA measurements show an abrupt in-plane spin-reorientation transition of the easy axis from  $[\bar{1}10]$  to  $[001]$  at a thickness,  $t_{\text{SRT}}$ . This thickness varied between samples from  $7.1 \text{ ML} \pm 0.3 \text{ ML}$  to  $7.4 \text{ ML} \pm 0.3 \text{ ML}$ . For thicknesses greater than  $t_{\text{SRT}}$ , the magnetization is parallel to  $[001]$ , consistent with previous studies of Co/GaAs(110). The domain structures above  $t_{\text{SRT}}$  were very different, with numerous irregularly shaped head-to-head domain walls. In addition, the region over which the reorientation occurred was unusually sharp, with a peak-to-peak spatial extent of only  $2.1 \mu\text{m} \pm 0.2 \mu\text{m}$ , which corresponded to a thickness change of  $0.28 \text{ ML} \pm 0.03 \text{ ML}$ . For Co wedges with a more gradual slope, the transition occurred over a smaller thickness range,  $0.16 \text{ ML} \pm 0.03 \text{ ML}$  in  $3.5 \mu\text{m} \pm 0.7 \mu\text{m}$ .

We do not believe that the spin-reorientation transition is due to the bcc to hcp phase transition, since the onset of the hcp-like phase occurred at different thicknesses for different samples, while  $t_{\text{SRT}}$  remained the same. This claim is further supported by the fact that the NRL group observed a structural transition from bcc to hcp without the presence of a spin-reorientation transition.<sup>2</sup>

The existence of a ferromagnetic phase between  $t_{\text{onset}}$  and  $t_{\text{SRT}}$ , with an easy axis along  $[\bar{1}10]$ , is consistent with an

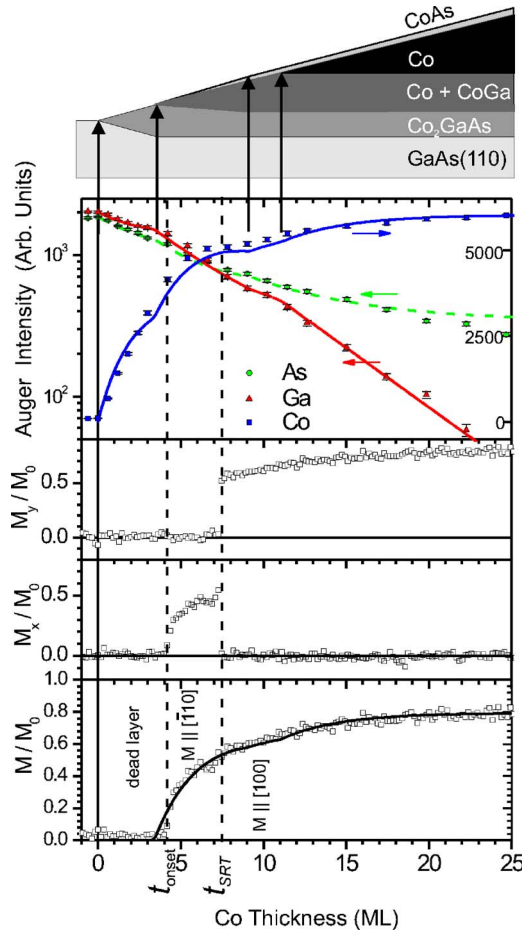


FIG. 3. (Color online) Top: Auger intensities as a function of Co thickness with a sketch of the model used to fit the data. The Auger data is taken from the differentiated signals from the Co 773 eV, the Ga 1064 eV, and the As 1223 eV peaks. The Ga and As data is plotted on a logarithmic scale, while the Co data is displayed on a linear scale to emphasize the feature at 9 ML. Middle:  $x$  and  $y$  magnetization components. Bottom: Total magnetization as a function of thickness. The solid lines in the top and bottom figures are calculated from fits to the growth model.

analysis of the surface anisotropies. In the case of a cubic material like Co, the anisotropy contains a cubic contribution,  $K_1^{\text{bulk}}$ . The lattice mismatch on the (110) surface yields a different strain along the  $[\bar{1}10]$  and  $[110]$  directions that gives rise to a magnetoelastic uniaxial contribution,  $K_u^{\text{bulk}}$ .<sup>18</sup> In addition, the nature of the bonding to the magnetically dead layer at the GaAs interface can give rise to surface anisotropies,  $K_1^{\text{interface}}$  and  $K_u^{\text{interface}}$ .<sup>19</sup> For an in-plane spin reorientation in the (110) plane, the surface and bulk anisotropies satisfy the following equation:<sup>20</sup>

$$K_1^{\text{interface}} + 4K_u^{\text{interface}} = t_{\text{SRT}}(K_1^{\text{bulk}} + 4K_u^{\text{bulk}}). \quad (1)$$

The anisotropies for a 35.7-nm-thick bcc-Co film are  $K_1 = -4.5 \times 10^4 \text{ J/m}^3$ , and  $K_u = 9.0 \times 10^4 \text{ J/m}^3$ , as measured by Brillouin light scattering.<sup>10</sup> Due to the large thickness of the film, the measured anisotropies may be used as good estimates of the bulk anisotropies. Substitution of these values,

and  $t_{\text{SRT}} = 7.3 \text{ ML}$  into Eq. (1), gives an estimate of the sum of the fourfold and uniaxial surface anisotropies,  $(K_1^{\text{interface}} + 4K_u^{\text{interface}}) = -0.46 \text{ mJ/m}^2$ . This is a reasonable value, as the anisotropy is comparable to the anisotropy  $(K_1^{\text{interface}} + 4K_u^{\text{interface}}) = -0.60 \text{ mJ/m}^2$  found for the Au/Fe/GaAs(110) systems.<sup>21</sup>

Scanning Auger microscopy provides insight into the evolution of the magnetic properties by mapping the chemical composition of the films along the wedge. Figure 3 shows a plot of the Co 773.6 eV, Ga 1064 eV, and As 1223 eV Auger electron intensities as a function of Co thickness. Several qualitative observations can be made from these data: the Ga and As signals initially decay slower, as a function of thickness, than would be expected from their associated mean free paths in Co of 1.62 nm and 1.80 nm, respectively. This suggests that Co initially intermixes with the GaAs. Co diffusion into the GaAs substrate is consistent with the delayed onset of the first RHEED intensity oscillation. After depositing 11 ML of Co, the Ga signal decreases at a rate consistent with Ga being buried under Co. The As signal, however, decays slowly after 11 ML, suggesting surface segregation of some of the As. And finally, the slope of the Co signal increases at 9 ML.

To make a more quantitative comparison with the magnetic data, we modeled the Auger data with the five layers shown in Fig. 3, CoAs/Co/(Co+CoGa)/Co<sub>2</sub>Ga<sub>x</sub>As<sub>1-x</sub>/GaAs. We calculated the Auger electron intensities for each element from their depth distributions by accounting for the exponential attenuation of the intensities with thickness.<sup>22</sup> The inelastic mean free paths were calculated from the formula of Tanuma *et al.*<sup>23</sup> We fitted the thickness dependence of all three Auger intensities simultaneously. The best fit indicated that the first 3.4 ML of Co reacted with the GaAs to create Co<sub>2</sub>Ga<sub>x</sub>As<sub>1-x</sub>, where  $x = 0.53 \pm 0.08$ . This is consistent with studies of Co/GaAs(100) annealed at a temperature of 375°C to form a Co<sub>2</sub>GaAs phase. This phase is orthorhombic and is well lattice matched to GaAs.<sup>15</sup>

The formation of Co<sub>2</sub>GaAs stops after 3.4 ML of deposition, as indicated by the abrupt change in slope in the Ga and As intensities. To model the Ga and As signals above this thickness, we allowed for CoGa diffusing into the Co film and CoAs segregating to the surface. The presence of CoGa and CoAs is supported by x-ray photoelectron spectroscopy (XPS) measurements.<sup>24</sup> Our model fit suggests that the top layer of the Co<sub>2</sub>GaAs diffused into the Co film; 0.86 ML  $\pm$  0.1 ML ( $1.5 \times 10^{19}$  atoms/m<sup>2</sup>) of CoAs segregated to the surface during the deposition of 3.4 ML to 9.1 ML of Co, and 0.97 ML  $\pm$  0.1 ML of CoGa diffused into the Co layer during the deposition from 3.4 ML to 11 ML. This corresponds to 6 at. % Ga in the Co film. We are not able to tell whether there is microphase separation or whether a homogeneous alloy is formed. Above 11 ML, a pure Co layer grew below the CoAs layer. The solid curves in Fig. 3 showed that this model provides reasonably good fits to the data. Better fits could be obtained by decreasing the Co mean free path by 5% to 1.215 nm, a value that is still consistent with the  $\pm 10\%$  uncertainty in the published inelastic mean free paths.

The Auger-based growth model quantitatively agrees with the observed magnetic properties of the film. Figure 3 shows

the total magnetization from the SEMPA measurements and the total magnetization calculated from the model. The first 3.4 ML, consisting primarily of Co<sub>2</sub>GaAs, are nonmagnetic. Co<sub>2</sub>GaAs is expected to be nonmagnetic, since both CoGa<sup>25</sup> and CoAs are nonmagnetic.<sup>26</sup> For thicknesses greater than 3.4 ML, we fit the total Co magnetization as a function of the thickness using the growth model. The fitting included a scaling factor and two fitting parameters: the spin scattering lengths through Co,  $\lambda_{\text{Co}}$ , and CoAs,  $\lambda_{\text{CoAs}}$ . The fits give  $\lambda_{\text{Co}}=0.70$  nm and  $\lambda_{\text{CoAs}}=1.2$  nm. The  $\lambda_{\text{Co}}$  is larger than a typical value of 0.5 nm for 3d transition metals.<sup>16</sup> This may be related to the nearly filled majority band in bcc-Co.

The growth model explains the magnetization well, except in a small region between 3.4 ML and  $t_{\text{onset}}=4.1$  ML where the measured magnetization is zero. RHEED measurements of Co island sizes, however, provide insight into this discrepancy. After 3.4 ML deposition, our model predicts that Co begins to nucleate on Co<sub>2</sub>GaAs. Analysis of the RHEED streaks estimates that the Co island separation is on the order of 6 nm. Islands of this size would be expected to

be superparamagnetic. The coalescence of these islands, presumably at  $t_{\text{onset}}=4.1$  ML, would explain the sudden jump in magnetization at this thickness.

In conclusion, we have observed three magnetic configurations in Co/GaAs(110). A dead layer is created at the Co/GaAs interface due to the formation of Co<sub>2</sub>GaAs. This observation confirms speculation in the literature that the decrease in the Co moment at the GaAs interface is due to Co reacting with the substrate. On top of this phase a bcc-Co film forms with 6 at. % Ga, with the easy axis along the  $[\bar{1}10]$  direction. The formation of the Co-Ga component marks the onset of ferromagnetism and leads to an in-plane spin-reorientation transition at higher film thickness.

This work was supported in part by the Office of Naval Research. T.L.M. would like to acknowledge financial support from the Natural Sciences and Engineering Research Council of Canada.

- 
- <sup>1</sup>C. S. Tian, D. Qian, D. Wu, R. H. He, Y. Z. Wu, W. X. Tang, L. F. Yin, Y. S. Shi, G. S. Dong, X. F. Jin, X. M. Jiang, F. Q. Liu, H. J. Qian, K. Sun, L. M. Wang, G. Rossi, Z. Q. Qiu, and J. Shi, *Phys. Rev. Lett.* **94**, 137210 (2005).
- <sup>2</sup>G. A. Prinz, *Phys. Rev. Lett.* **54**, 1051 (1985).
- <sup>3</sup>Y. U. Idzerda, W. T. Elam, B. T. Jonker, and G. A. Prinz, *Phys. Rev. Lett.* **62**, 2480 (1989).
- <sup>4</sup>P. C. Riedi, T. Dumelow, M. Rubinstein, G. A. Prinz, and S. B. Qadri, *Phys. Rev. B* **36**, 4595 (1987).
- <sup>5</sup>D. Bagayoko, A. Ziegler, and J. Callaway, *Phys. Rev. B* **27**, 7046 (1983).
- <sup>6</sup>J. I. Lee, C. L. Fu, and A. J. Freeman, *J. Magn. Magn. Mater.* **62**, 93 (1986).
- <sup>7</sup>G. A. Prinz, E. Kisker, K. B. Hathaway, K. Schröder, and K.-H. Walker, *J. Appl. Phys.* **57**, 3024 (1985).
- <sup>8</sup>J. P. Velev, K. D. Belashchenko, D. A. Stewart, M. van Schilf-gaarde, S. S. Jaswal, and E. Y. Tsybal, *Phys. Rev. Lett.* **95**, 216601 (2005).
- <sup>9</sup>S. Yuasa, T. Katayama, T. Nagahama, A. Fukushima, H. Kubota, Y. Suzuki, and K. Ando, *Appl. Phys. Lett.* **87**, 222508 (2005).
- <sup>10</sup>X. Liu, R. L. Stamps, R. Sooryakumar, and G. A. Prinz, *J. Appl. Phys.* **79**, 5387 (1996).
- <sup>11</sup>J. A. C. Bland, R. D. Bateson, P. C. Riedi, R. G. C. Graham, H. J. Lauter, J. Penfold, and C. Shackleton, *J. Appl. Phys.* **69**, 4989 (1991).
- <sup>12</sup>K. G. Nath, F. Maeda, S. Suzuki, and Y. Watanabe, *J. Appl. Phys.* **91**, 3943 (2002).
- <sup>13</sup>M. Izquierdo, M. E. Davila, J. Avila, H. Ascolani, C. M. Teodor-escu, M. G. Martin, N. Franco, J. Chrost, A. Arranz, and M. C. Asensio, *Phys. Rev. Lett.* **94**, 187601 (2005).
- <sup>14</sup>F. Xu, J. J. Joyce, M. W. Ruckman, H.-W. Chen, F. Boscherini, D. M. Hill, S. A. Chambers, and J. H. Weaver, *Phys. Rev. B* **35**, 2375 (1987).
- <sup>15</sup>C. J. Palmstrom, C. C. Chang, A. Yu, G. J. Galvin, and J. W. Mayer, *J. Appl. Phys.* **62**, 3755 (1987).
- <sup>16</sup>D. T. Pierce, J. Unguris, and R. J. Celotta, *Ultrathin Magnetic Structures* (Springer-Verlag, New York, 1994), pp. 117–147.
- <sup>17</sup>G. A. Prinz, *Ultrathin Magnetic Structures* (Springer-Verlag, New York, 1994), pp. 1–44.
- <sup>18</sup>S. Subramanian, X. Liu, R. L. Stamps, R. Sooryakumar, and G. A. Prinz, *Phys. Rev. B* **52**, 10194 (1995).
- <sup>19</sup>J. J. Krebs, B. T. Jonker, and G. A. Prinz, *J. Appl. Phys.* **61**, 2596 (1987).
- <sup>20</sup>U. Gradmann, J. Korechi, and G. Waller, *Appl. Phys. A* **39**, 101 (1986).
- <sup>21</sup>R. Höllinger, M. Zöfl, R. Moosbühler, and G. Bayreuther, *J. Appl. Phys.* **89**, 7136 (2001).
- <sup>22</sup>M. P. Seah, in *Practical Surface Analysis*, edited by B. Briggs and M. P. Seah (John Wiley and Sons, Ltd., West Sussex, 1983), p. 244.
- <sup>23</sup>S. Tanuma, C. J. Powell, and D. R. Penn, *Surf. Interface Anal.* **17**, 911 (1991).
- <sup>24</sup>K. Lüdige, D. B. Schultz, P. Vogt, M. M. R. Evans, W. Braun, C. J. Palmstrom, W. Richter, and N. Esser, *J. Vac. Sci. Technol. B* **20**, 1591 (2002).
- <sup>25</sup>A. Amamou and F. Gautier, *J. Phys. F: Met. Phys.* **4**, 563 (1974).
- <sup>26</sup>K. Selte and A. Kjekshus, *Acta Chem. Scand.* (1947-1973) **25**, 3277 (1971).